



Extremely low efficiency roll-off of phosphorescent organic light-emitting diodes at high-brightness based on acridine heterocyclic derivatives

Journal:	<i>Journal of Materials Chemistry C</i>
Manuscript ID	TC-ART-06-2018-002739.R1
Article Type:	Paper
Date Submitted by the Author:	22-Jul-2018
Complete List of Authors:	Chen, Minyu; Key Laboratory of Advanced Display and System Applications, Ministry of Education, Shanghai University Yang, Jiali; Shanghai University Ye, Zhonghua; Shanghai University Wang, Shuang long; Shanghai University Tang, Zhenyu; Shanghai University Chen, Guo; Shanghai University, Key Laboratory of Advanced Display and System Applications Zheng, Yanqiong; Key Laboratory of Advanced Display and System Applications, Ministry of Education, Shanghai University Shi, Ying; School of Material Science and Engineering, Shanghai University Wei, Bin; Key Laboratory of Advanced Display and System Applications, Ministry of Education, Shanghai University, Wong, Wai-Yeung (Raymond); The Hong Kong Polytechnic University, Faculty of Applied Science and Textiles



Journal Name

ARTICLE

Extremely low efficiency roll-off of phosphorescent organic light-emitting diodes at high-brightness based on acridine heterocyclic derivatives†

Received 00th January 20xx,
Accepted 00th January 20xx

DOI: 10.1039/x0xx00000x

www.rsc.org/

Minyu Chen^{‡a}, Jiali Yang^{‡a}, Zhonghua Ye^b, Shuanglong Wang^a, Zhenyu Tang^a, Guo Chen^a, Yanqiong Zheng^a, Ying Shi^{b*}, Bin Wei^{a*}, Wai-Yeung Wong^{c*}

Three novel host materials, IpCm-PhBzAc (1,3-(4-(12,12-dimethylbenzofuro[3,2-b]acridin-7(12H)-yl)phenyl)-6-isopropyl-4H-chromen-4-one), DpAn-BzAc (2,10-(4-(12,12-dimethylbenzofuro[3,2-b]acridin-7(12H)-yl)phenyl)-10-phenylanthracen-9(10H)-one) and DpTrz-BphBzAc (3,7-(4'-(4,6-diphenyl-1,3,5-triazin-2-yl)-[1,1'-biphenyl]-4-yl)-12,12-dimethyl-7,12-dihydrobenzofuro[3,2-b]acridine) have been designed and synthesized, and their utilization as host materials for phosphorescent organic light-emitting diodes (PhOLEDs) have been investigated. We have fabricated PhOLEDs using green bis(2-phenylpyridine)iridium(III) acetylacetonate as doped emitters and two hosting schemes, which are the single host system consisting of BzAc derivatives and the cohost system with 1,3-bis(carbazolyl)benzene. We found that the PhOLEDs with co-host system of DpAn-BzAc and DpTrz-BphBzAc achieved CE of 57.1 cd A⁻¹ and 53.0 cd A⁻¹, with the corresponding efficiency roll-off of only 7.6% and 0.9%, respectively, from the maximum to the practical brightness of 5000 cd m⁻². The extremely reduced efficiency roll-off for BzAc-based PhOLEDs were attributed to the superior thermal stability and excellent bipolar transport properties, and a small singlet-triplet energy gap also afforded efficient reverse intersystem crossing, thus reducing the triplet density of the host for PhOLEDs.

Introduction

Organic light-emitting diodes (OLEDs) have attracted increasing attention in scientific and industrial research because of the promising applications in display and solid state lighting.¹⁻³ Phosphorescent OLEDs (PhOLEDs) have been widely used in high-brightness lighting and biological probe owing to their full utilization of singlet and triplet excitons to provide high electroluminescence (EL) efficiency.⁴⁻⁵ To achieve the full commercialization of OLEDs in lighting and fluorescence sensing applications,⁶⁻⁷ it is believed that the improvements of thermal stability and the mitigation of efficiency roll-off are important.

To date, most researchers have already achieved high efficiency OLEDs with a low efficiency roll-off at a luminance of

1000 cd m⁻². Su et al reported a nondoped OLED based on a new tailor-made luminophor that provided excellent peak EL efficiencies of 43.3 cd A⁻¹, with an extremely small current efficiency roll-off of 0.46% at 1000 cd m⁻².⁸ Liu et al. fabricated a series of simplified trilayer PhOLEDs with high efficiency and little efficiency roll-off based on a bipolar iridium emitter which can help balance charge fluxes and contribute to direct exciton formation in the EMLs.⁹ Hung et al. demonstrated that high efficiency and low roll-off can be achieved in a carrier- and exciton-confined device structure.¹⁰ At a practical brightness of 1000 cd m⁻², this device performance (EQE) remained as high as 16.7% (the maximum value is 18.3%). Nevertheless, the efficiency roll-off of the aforementioned OLEDs at the high-brightness region over 5000 cd m⁻² is still large.

The roll-off phenomenon is mainly caused by triplet-triplet annihilation (TTA) originating from the long lifetime of the triplet excited state and triplet-polaron quenching (TPQ), which limits the current efficiency of PhOLEDs at high current density.¹¹⁻¹² To realize efficient PhOLEDs and reduced efficiency roll-off at the high-brightness region, it has been known that the approaches are effective by reducing molecular aggregation, broadening the recombination zone, decreasing the exciton lifetime and suitable triplet management.¹³

^a School of Mechatronic Engineering and Automation, Key Laboratory of Advanced Display and System Applications, Ministry of Education, Shanghai University, 149 Yanchang Road, Shanghai, 200072, P. R. China.

^b School of Materials Science and Engineering, Shanghai University, Shanghai 200072, P. R. China.

^c Department of Applied Biology and Chemical Technology, The Hong Kong Polytechnic University, Hung Hom, Hong Kong, P. R. China.

† Electronic Supplementary Information (ESI) available: 1H NMR spectra, CV curves, TGA and DSC, absorption and emission spectra of complexes, as well as synthesis of intermediates, AFM images and EL spectra, CIE coordinates of devices A-2, B-2 and C-2. See DOI: 10.1039/x0xx00000x

‡ These authors contributed equally to this work *Email - bwei@shu.edu.cn

The homogeneous dispersion of the phosphors in a suitable host matrix is crucial for reducing concentration quenching and triplet-triplet annihilation, which is detrimental to the efficiency roll-off.¹⁴ Recently, a potential approach is to use materials with thermally activated delayed fluorescence (TADF) as a host for giving low roll-off OLEDs, due to the excitons upconverted from long-lifetime triplet state to short-lifetime singlet state via reverse intersystem crossing (RISC) process.¹⁵ The utilization of triplet excitons by the TADF mechanism became an optional approach for organic complexes in OLEDs with limited roll-off efficiency. Furthermore, the host materials also play an important role for carrier transport and charge balance. Recently, bipolar materials as hosts have gained immense interests for optoelectronic applications.¹⁶⁻¹⁹ Improvement of carrier mobility and balance of electrons and holes by using the bipolar host are essential for reducing the driving voltage and increasing the current and power efficiencies.²⁰ Then, a low operating voltage will generate less heat, reducing crystallization and destruction of the surface topography of the material, which will mitigate the roll-off of efficiency at high brightness.

Following this consideration, a rational molecular structure design strategy to obtain efficient bipolar TADF materials was presented to combine an electron-donating and -withdrawing functionality in a twisted molecular framework.²¹⁻²³ The acridine-based moieties, which possess excellent electron donating ability and high thermal stability, are better than carbazole-type moieties as the donors of efficient TADF materials.²⁴⁻²⁶ Ketones and the triazine units can be applied as acceptors to the bipolar molecules, due to their strong electron withdrawing properties, good thermal and chemical stabilities.²⁴ A small splitting of singlet and triplet (ΔE_{ST}) can be achieved by a twisted connection between the donor and acceptor moieties, causing the spatial separation of the electron densities of the frontier orbitals.²⁷⁻²⁸

Moreover, besides molecular designs for the host, structure designs for the emitting layer (EML) have been employed to enhance the performance of high-brightness PhOLEDs. Employing a mixed host should balance charge carriers, facilitate the recombination probability of electrons and holes, and inhibit crystallization of EML, as an effective device structure to generate highly efficient PhOLEDs with low efficiency roll-off.²⁹ For example, Kim et al. developed a fac-tris (2-phenylpyridine) iridium (III) [Ir(ppy)₃]-based green OLED with 10% roll-off of the current efficiency at a luminance of 20000 cd m⁻² by adopting a mixed host to balance charge carriers in the EML and broaden the recombination zone.³⁰

In this paper, we report three host compounds (IpCm-PhBzAc, DpAn-BzAc and DpTrz-BphBzAc) based on the 12,12-dimethyl-7,12-dihydrobenzofuro[3,2-b]acridine (BzAc) donor unit with different acceptors. DpAn-BzAc and DpTrz-BphBzAc exhibited a small ΔE_{ST} , affording efficient RISC, and TADF features. Bis(2-phenylpyridine)iridium(III) acetylacetonate [(ppy)₂Ir(acac)] was doped in this TADF host, and high efficiency green PhOLEDs with low turn-on voltage of 2.2 V and 2.3 V were achieved. In particular, the DpTrz-BphBzAc-based device showed extremely low drive voltage of 4.5 V at 10000 cd m⁻².

In addition, by mixing 1,3-bis(carbazolyl)benzene (mCP) and new materials as the host, the best PhOLED presented a high current efficiency of 53.5 cd A⁻¹ with an extremely small current efficiency roll-off of 0.9% at 5000 cd m⁻² by reducing the triplet density on the host and thus diminishing the TTA and TPA.

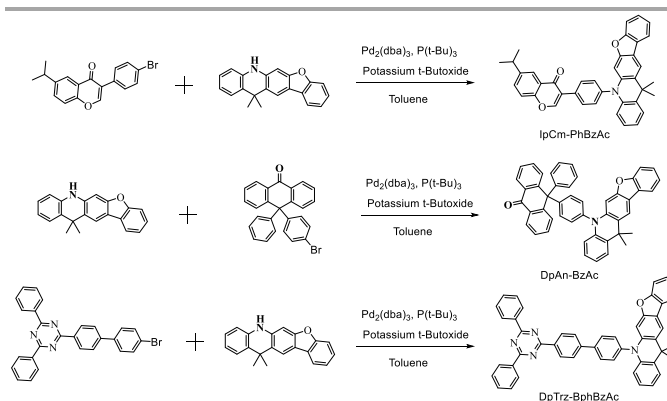
Results and discussion

Synthetic scheme

The synthetic routes toward the host materials IpCm-PhBzAc, DpAn-BzAc and DpTrz-BphBzAc are illustrated in Scheme 1. The synthesis of intermediates for 3-(4-bromophenyl)-6-isopropyl-4H-chromen-4-one (PhBzAc), 3-(4-bromophenyl)-6-isopropyl-4H-chromen-4-one (IpCm) and 2-(4'-bromo-[1,1'-biphenyl]-4-yl)-4,6-diphenyl-1,3,5-triazine (DphTrz) followed the literature procedure.³¹⁻³³ The ancillary ligand 10-(4-bromophenyl)-10-phenylanthracen-9(10H)-one (DphAn-Br) was readily synthesized from 10H-spiro[anthracene-9,2'-[1,3]dioxolan]-10-one and 10,10-diphenyl-10H-spiro[anthracene-9,2'-[1,3]dioxolane]. The target compounds IpCm-PhBzAc, DpAn-BzAc and DpTrz-BphBzAc were obtained by the Buchward-Hartwig coupling reaction between corresponding intermediates and ancillary ligands in toluene. The details for the preparation and ¹H NMR spectra of these compounds are given in the experimental section and supporting information (Scheme.S1 and Fig.S1, in the ESI[†]).

Theoretical calculations

Molecular simulations were carried out to better understand the structural properties of our designed host materials. The three-dimensional geometry and the frontier molecular orbital energy levels of the three complexes were calculated using density functional theory (DFT) at the B3LYP/6-31G* level. Fig. 1 depicts the frontier molecular orbital distribution of the HOMOs and LUMOs for the compounds. The HOMOs of the molecules are mainly located on electron-donating BzAc moiety, while the LUMOs are concentrated on the electron-withdrawing IpCm, PnAn and triazine moieties, respectively. Almost no overlap between the HOMO and LUMO for all the host materials can be observed due to the effective separation of the electron densities, which enables a small ΔE_{ST} and accelerates the reverse intersystem crossing (RISC).



Scheme 1 Molecular structures and synthesis of the target compounds IpCm-PhBzAc, DpAn-BzAc and DpTrz-BphBzAc.

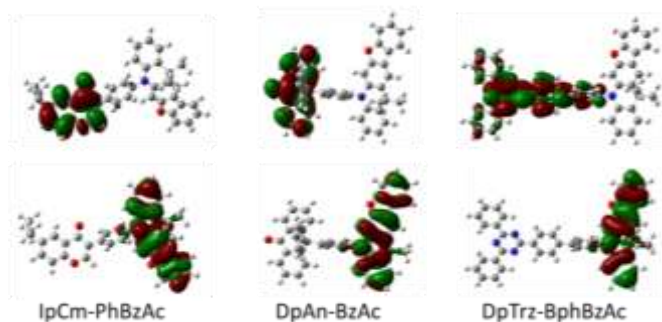


Fig. 1 HOMO (bottom) and LUMO (top) of IpCm-PhBzAc, DpAn-BzAc and DpTrz-BphBzAc as computed in Gaussian 09 DFT B3LYP/6-31G* level of theory.

Electrochemical properties

The electrochemical properties of synthesized compounds were determined by cyclic voltammetry in THF solution. As shown in Fig. S2 (in the ESI[†]), each of these three compounds displayed oxidation with the oxidative signal at ~ 0.50 V, indicating the formation of stable cation radical under the electrochemical condition, which was attributed to the BzAc unit. Among these three materials, the narrower oxidation peak width of DpAn-BzAc demonstrated the preferable chemical stability, which is beneficial to the efficiency enhancement of the device. The HOMOs were determined using photoelectron spectroscopy. Notably, all HOMOs were shallower than that of the carbazole compound (ca. 6.0 eV) due to the strong electron-donating character of the BzAc moiety.

Photophysical properties

The absorption and photoluminescence (PL) spectra of IpCm-

Table 1 Summary of the physical properties of IpCm-PhBzAc, DpAn-BzAc and DpTrz-BphBzAc.

	IpCm-PhBzAc	DpAn-BzAc	DpTrz-BphBzAc
$T_g/T_d/T_m$ (°C)	109/421/203	137/394/345	148/427/279
HOMO/LUMO (eV) ^a	-5.6/-2.4	-5.6/-2.3	-5.7/-2.9
E_T (eV) ^b	2.70	2.71	2.68
ΔE_{ST} (eV) ^c	0.35	0.38	0.17
λ_{max}^{abs} (nm) ^d	345	348	310
λ_{max}^{PL} (nm) film ^e /sol ^d	449,476/454	524/433	496/484
τ^e	6.6 ns /---	402 ns/3.39 μ s	71 ns/0.35 μ s
PLQY ^e	13.7%	76.3%	90.3%

^a HOMO was determined using photoelectron spectroscopy.

LUMO = HOMO + E_g where E_g is the optical band gap in film.

^b Triplet energy corresponding to the first vibronic band of the phosphorescence spectra in frozen toluene (77 K).

^c ΔE_{ST} = energy gap between S_1 and T_1 .

^d In toluene solution.

^e Neat films were made on quartz substrates with a thickness of about 60 nm.

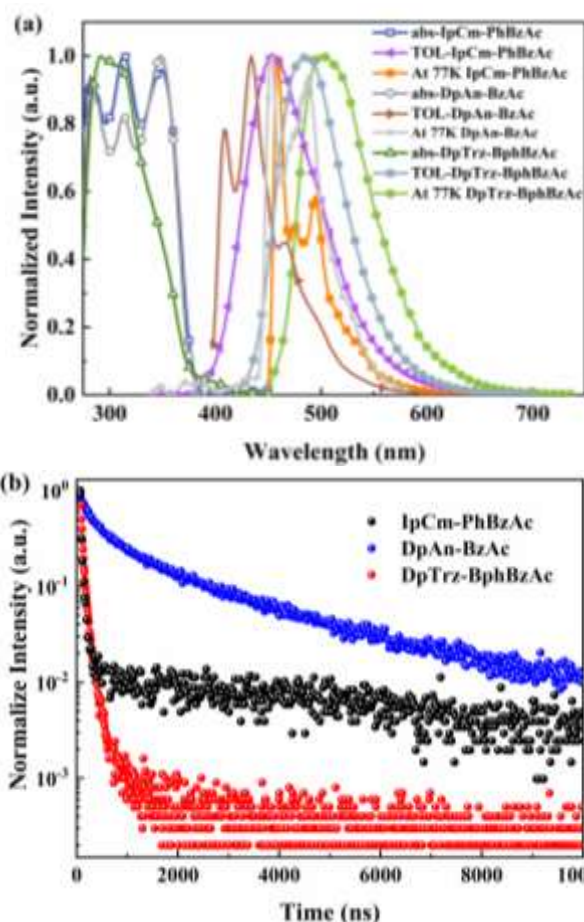


Fig. 2 (a) UV-vis absorption (Abs) and PL spectra of IpCm-PhBzAc, DpAn-BzAc and DpTrz-BphBzAc in thin solid film at room temperature and low temperature; (b) the transient decay curve of IpCm-PhBzAc, DpAn-BzAc and DpTrz-BphBzAc film at room temperature.

PhBzAc, DpAn-BzAc and DpTrz-BphBzAc in TOL are shown in Fig. 2, and the detailed photophysical characterization data are summarized in Table 1. The compounds exhibited π - π^* transitions below 300 nm, and n - π^* transitions between 300 and 350 nm in the UV-vis absorption spectra. The maximum PL emission wavelengths of IpCm-PhBzAc, DpAn-BzAc and DpTrz-BphBzAc were observed at 454, 433 and 496 nm in toluene solution at room temperature.

By comparison with its UV-vis absorption spectra, big Stokes shifts were observed, which means that the compounds have more geometrical change and intramolecular charge transfer in the excited state. The PL emission of acridine heterocyclic derivatives overlap well with the UV-vis absorption of the metal to ligand charge transfer (MLCT) for the Ir-complex, suggesting efficient Förster energy transfer from the hosts to the emitter (Fig. S3, in the ESI[†]). The phosphorescence spectra of the materials were measured in toluene solution at low temperature (77 K, in liquid nitrogen), which can be considered to better estimate the triplet energy of the host from the highest energy vibronic band. Thus, the triplet energies of the three hosts are found to be 2.7 eV, 2.71 eV and 2.68 eV, which are sufficient to host green phosphorescent

dopants. The energy levels and photophysical properties of IpCm-PhBzAc, DpAn-BzAc and DpTrz-BphBzAc were investigated in toluene. The phosphorescent spectra of IpCm-PhBzAc and DpAn-BzAc show well defined vibronic structures in toluene at 77 K, indicating that their lowest triplet states are LE states. Following the reported results³⁴, the ΔE_{ST} of IpCm-PhBzAc, DpAn-BzAc and DpTrz-BphBzAc in toluene were calculated to be 0.35, 0.38 and 0.19 eV, respectively, which gives the possibility for the efficient RISC from T_1 to S_1 under thermal activation, demonstrating the TADF potential in neat films. To gain an insight into the photophysical process, the transient fluorescence behaviors of neat films of the compounds were investigated. As shown in Fig. 2b and Fig. S4 (in the ESI[†]), the transient PL decay spectra of both DpAn-BzAc and DpTrz-BphBzAc follow a double exponential model comprised of a prompt component and a delayed component. At ambient temperature (300 K), the neat film of DpAn-BzAc has a prompt fluorescence decay time of 402 ns and a delayed fluorescence decay time of 3.39 μ s, and the transient decay times of DpTrz-BphBzAc were estimated to be 71 ns and 0.35 μ s for the prompt component and the delayed component. The shorter delayed fluorescence decay time of DpTrz-BphBzAc inspired a more stable device. A single exponential of the fluorescence lifetime of IpCm-PhBzAc can be observed which verifies a pure excited state with the prompt fluorescence decay. Although the ΔE_{ST} of IpCm-PhBzAc is only 0.35 eV, it is possible that the difference between 3CT and 3LE of IpCm-PhBzAc is relatively large, as schematically shown in Fig. S5 (in the ESI[†]), which limits the up-conversion of exciton on 3LE , thus RISC will not happen. In addition, the PL quantum yields (PLQYs) of IpCm-PhBzAc, DpAn-BzAc and DpTrz-BphBzAc were 13.7%, 76.3% and 90.3%, implying their promising applications in electrophosphorescence.

Thermal properties

Thermal and morphological stabilities are necessary to fabricate efficient OLEDs with higher operational stability. At high brightness, the nonradiative emission in the device is also increased due to the rise of the operating voltage of the device. The good thermal stability of the host material could ensure effectively good film-forming properties and reduce the phase separation, thereby alleviating the roll-off of device efficiency under high brightness. Thermal properties are examined by thermal gravimetric analysis (TGA) and differential scanning calorimetry (DSC). As displayed in Fig. S6 (in the ESI[†]), and Table 1, the decomposition temperatures (5% loss of weight) are 202 $^{\circ}C$ for IpCm-PhBzAc, 344 $^{\circ}C$ for DpAn-BzAc and 353 $^{\circ}C$ for DpTrz-BphBzAc, respectively, indicating that DpAn-BzAc and DpTrz-BphBzAc are more stable than IpCm-PhBzAc. The DSC results indicate that both DpAn-BzAc and DpTrz-BphBzAc exhibit the high T_g of 136 $^{\circ}C$ and 148 $^{\circ}C$, which is promising for serving as the host materials in terms of morphological stability in the device.

The AFM images further illustrates the thermal stability and surface appearance. Figure 3 and Fig. S7 (in the ESI[†]) compare the topography of the host films under different temperatures. For DpAn-BzAc, the roughness changed from 0.71 nm at room temperature to 0.416 nm at 100 $^{\circ}C$. The morphology of DpAn-BzAc seemed much flatter and improved its PLQY. However, at a higher temperature (200 $^{\circ}C$), the crystallized material can be observed. Simultaneously, the PL spectrum of the film was deformed and the PLQY dropped to 13.45%. In particular,

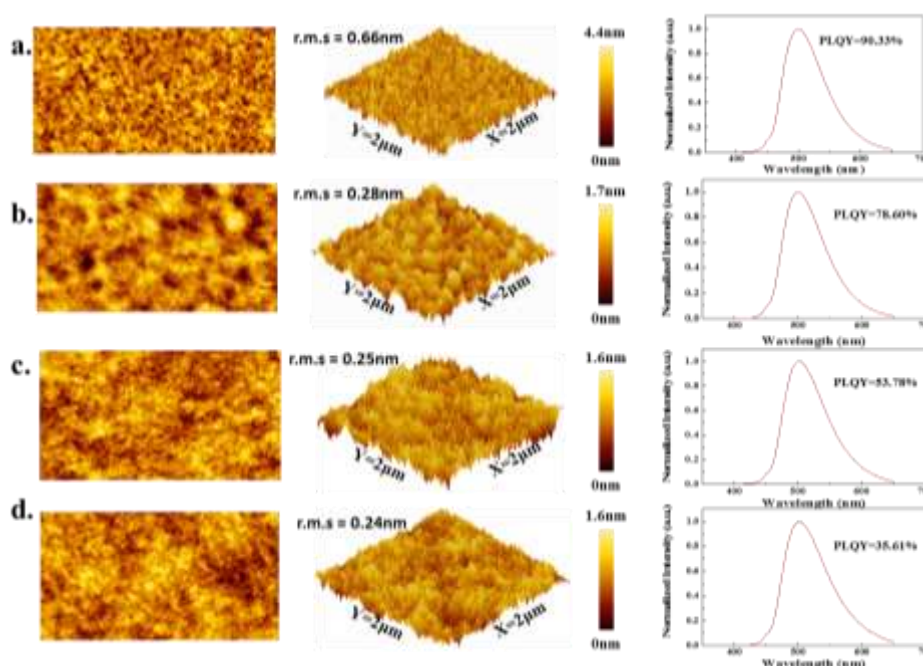


Fig 3. (a-d) AFM characterization and PL spectra. Height images (left), three-dimensional images (middle) and PL spectra (right) of DpTrz-BphBzAc films at room temperature (a) and under 100 $^{\circ}C$ (b); 200 $^{\circ}C$ (c); 300 $^{\circ}C$ (d) annealing temperatures (20 minutes).

when the temperature rose to 300 °C, the luminescence was completely quenched, as verified by the PLQY being 0%. For DpTrz-BphBzAc, the 4,6-diphenyl-1,3,5-triazine-substituted BzAc groups kept much better morphology than DpAn-BzAc at a very high annealing temperature, 300 °C, with the roughness changing from 0.66 nm to only 0.28 nm. Obviously, even at 300 °C, the PL spectrum of the DpTrz-BphBzAc did not undergo significant deformation, and PLQY remained at 35.6%, exhibiting an extraordinary thermally stable luminescence.

Carrier mobilities

The highly efficient carrier mobility of the materials is crucial to facilitate the injection and transport of charge carriers and balance the hole–electron distribution, which lead to suppressed TTA and TPQ effects, improved recombination probability, high device efficiency, and low efficiency roll-off.^{35–36} In order to evaluate the carrier-transporting properties of the title compounds, hole-only (HOD) and electron-only devices (EOD) were fabricated. The construction of the hole-only device is ITO/HAT-CN (10 nm)/TAPC (20 nm)/host (20 nm)/TAPC (20 nm)/HAT-CN (10 nm)/Al (100 nm), and the electron-only device is ITO/TPBi (30 nm)/host (20 nm)/TPBi (30 nm)/Liq (1 nm)/Al (100 nm). The *J-V* plots (Fig. 4) shows that the current densities of hole-only devices based on BzAc derivatives are visibly higher than that of the popular host

material mCP due to the preferable electron-donating property of BzAc moiety. The electron mobilities for the compounds follow the orders of DpTrz-BphBzAc > IpCm-PhBzAc \approx DpAn-BzAc > mCP. We have noticed that DpTrz-BphBzAc has the highest current densities in EODs, demonstrating a higher electron-transporting property of the triazine as the electron acceptor unit. In addition, since the EOD of DpTrz-BphBzAc has a larger *J-V* curve growth rate than HOD, the charge carrier mobilities will remain balanced in the material when the voltage reaches a certain value, indicating a better bipolar property of DpTrz-BphBzAc. Among these compounds, DpTrz-BphBzAc has the appropriate hole and electron current densities in both HOD and EOD, suggesting a more stable performance at high luminance that could be expected at the device level.

Electroluminescence properties

The OLED structure was: indium tin oxide (ITO)/HAT-CN (10 nm)/NPB (50 nm)/TAPC (60 nm)/12 wt% (ppy)₂Iracac: IpCm-PhBzAc (device A1) or 12 wt% (ppy)₂Iracac: DpAn-BzAc (device B1) or 12 wt% (ppy)₂Iracac: DpTrz-BphBzAc (device C1) (40 nm)/TPBi :TmPyPb(1:1 35 nm)/Liq (1 nm)/Al (100 nm), where HAT-CN was employed as the hole injection layer (HIL), (NPB) and TAPC were used as the hole transport layers (HTLs), and TPBi and TmPyPB were applied to the electron transport layer (ETL). Fig. 5 shows the schematic diagram of the device structure. The introduction of the TmPyPB and TPBi mixing layer did not only act as an electron transporter, but also plays a significant role in blocking carriers, by which we confine excitons in the EML for avoiding the energy outflow.

The electroluminescence (EL) spectra and potential (*V*)–luminance (*L*), current density (*J*)–current efficiency (CE) and current density (*J*)–external quantum efficiency (EQE) curves of the OLEDs based on the title materials are depicted in Fig. 6. The EL emission peaks at 524, 527 and 524 nm for devices A1, B1 and C1, respectively, which shows that all of the devices emit green light with the similar emission wavelength from (ppy)₂Iracac, due to the effective confinement of the triplet excitons within the emitting layer. No other residual emission bands from the host and/or adjacent layers indicate that the energy transfer from the host to the guest is complete.

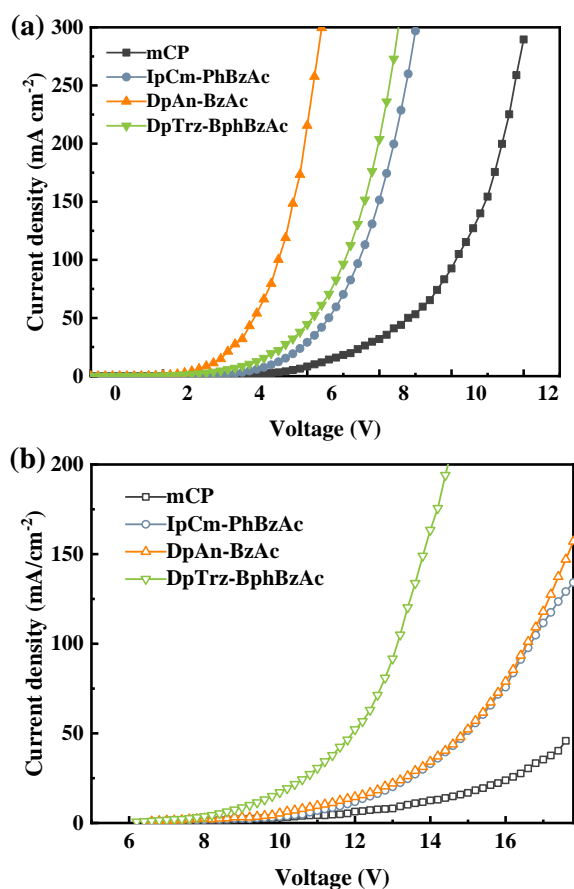


Fig. 4 *J-V* characteristics of (a) hole-only and (b) electron-only devices for mCP, IpCm-PhBzAc, DpAn-BzAc and DpTrz-BphBzAc.

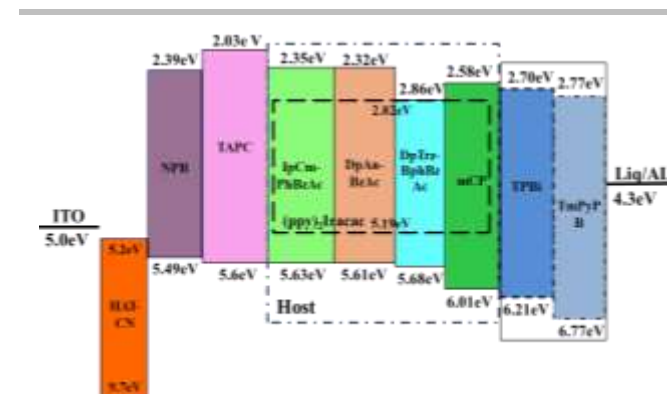


Fig. 5 Energy level diagram of the OLED.

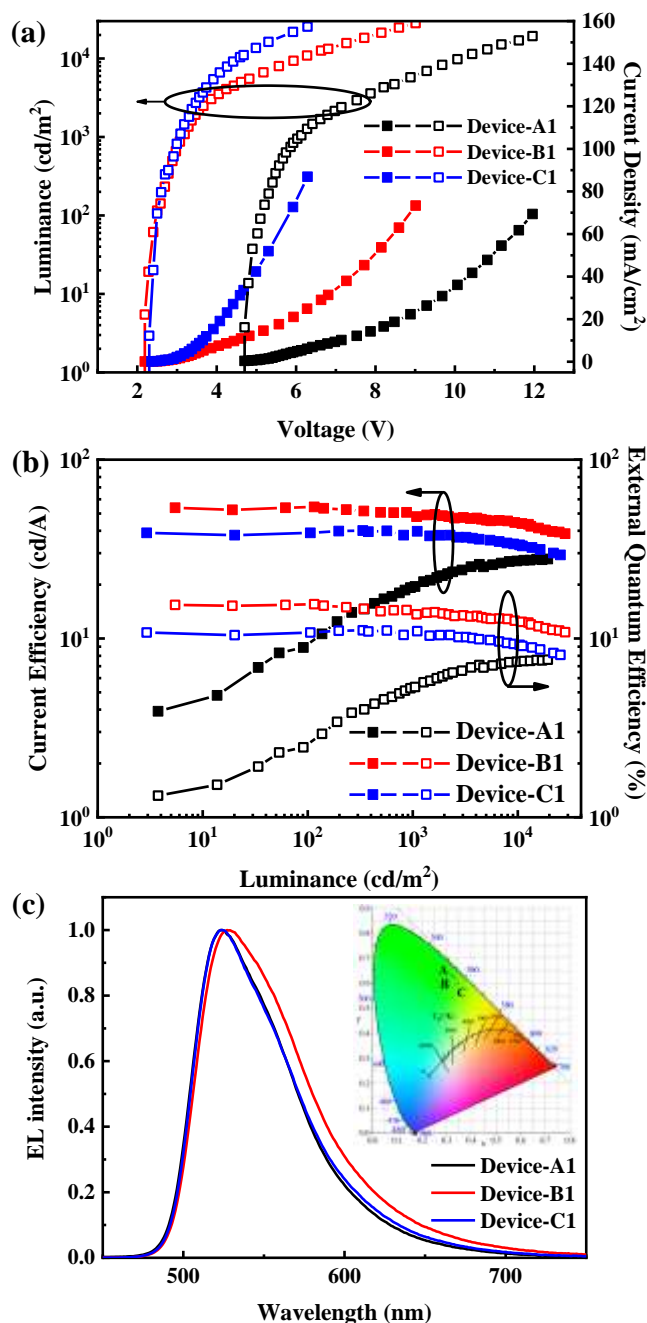


Fig. 6 a) Luminance–voltage–current density. b) current efficiency–luminance–EQE characteristics. c) EL spectra at 1000 cd m⁻². Inset: CIE coordinates of devices A1, B1 and C1.

Devices with DpAn-BzAc and DpTrz-BphBzAc as hosts exhibit much higher efficiencies than the IpCm-PhBzAc hosted device, which are consistent with the PLQY (Table. 1). The turn-on voltages at 1 cd m⁻² of device B1 and device C1 are 2.2 V and 2.3 V, which approximately match with the photon energy of emitter (ppy)₂Iracac. The DpAn-BzAc based device B1 reached the highest efficiency, with a peak current efficiency (CE) of 54.4 cd A⁻¹, a maximum forward viewing external quantum efficiency (EQE) of 15.5%, and a peak power efficiency (PE) of 70.4 lm W⁻¹. As shown in Fig. 5, the LUMO of the electron transport layer and the Ir complex are similar, indicating that the

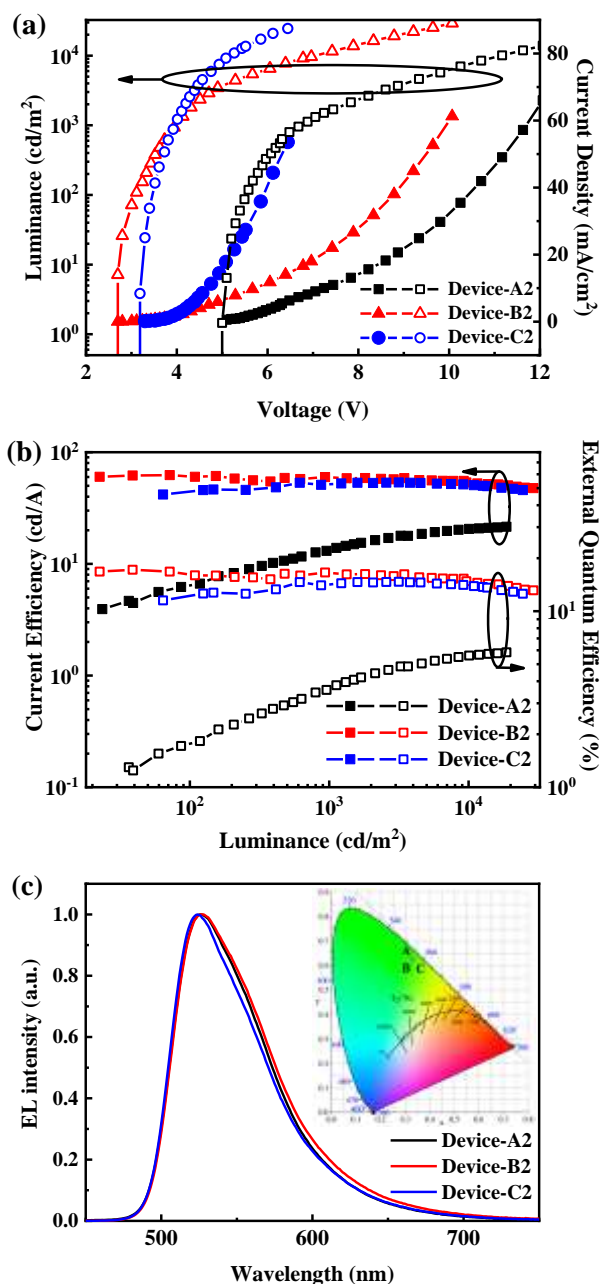
electrons are directly captured by the dopant. Whereas the holes are transported from the transport layer through the host to the dopant due to the difference between the HOMOs of the hole transport layer and the guest. In this case, the transport capability of holes is affected by the mobility of the host material. As shown in the hole-only device (Fig. 4), the hole mobility of the DpAn-BzAc is greater than that of the DpTrz-BphBzAc. Therefore, the turn-on voltage of DpAn-BzAc is lower. In addition, we measured the PLQY of the doped films. Result shows that DpAn-BzAc doped (ppy)₂Iracac film has a higher PLQY of 61.7%, while the DpTrz-BphBzAc doped (ppy)₂Iracac film has only 58.7%. The more efficient energy transfer process from DpAn-BzAc to dopant is consistent with the superior performance of the device based on DpAn-BzAc. The superior performance of the device B1 is consistent with the higher PLQY (61.7%) of DpAn-BzAc doped film than DpTrz-BphBzAc doped one (58.7%), which provide a more efficient energy transfer process from host to dopant. Although the efficiencies of device C1 are inferior to those with the device B1, the operational stability is better. Notably, the efficiency roll-off of device C1 is low with CE of 39.3 cd A⁻¹ at 1000 cd m⁻², 35.8 cd A⁻¹ at 5000 cd m⁻² and 33.3 cd A⁻¹ at 10000 cd m⁻², respectively. These reduced roll-off effect are, most likely, results of superior TADF characteristic to reduce the excitation of T₁ state by prompt RSIC process of DpTrz-BphBzAc. In addition, the operating voltage of device C1 at 10000 cd m⁻² is as low as 4.5 V, which is ascribed to the efficient electron-hole capture at high doping concentration with less additional carrier injection barrier and carrier balance in EML by the preferable bipolar material and the optimized structure.

To improve the EL efficiencies and reduce the roll-off of devices, we attempted to use a co-host system in EML. By introducing mCP as co-host, the recombination zone can be broadened, which is beneficial to reduce the triplet exciton density, thereby alleviating the TTA and TPQ at high currents. Furthermore, the mCP with high triplet energy and the low HOMO level can effectively confine the triplet excitons on the dopant molecules and prevent the excess holes from TPBi. In addition, co-host system provides the carrier with an additional hopping energy level channel, which helps to reduce the accumulation of excitons at the interface. Hence, we used mCP and new materials as co-hosts with the mass ratio of 1:1. (ppy)₂Iracac was the dopant at 12%.

Device performance data are summarized in Fig. 7 and Table 2. As expected, the performance of co-host devices B2 and C2 are superior to those with single host devices. The DpAn-BzAc based co-host device B2 revealed the highest CE of 61.8 cd A⁻¹ and the maximum EQE of 17.2%. For device C2, a CE_{max} of 53.5 cd A⁻¹ and a EQE_{max} of 14.7% were achieved. We attribute the superior performance of the two co-host devices to a recombination zone that is distributed over the entire emitter layer and to the less leakage of exciton. Interestingly, the introduction of mCP in EML led to a drop in the efficiency of device A2. The probable cause is the poorer PLQY of IpCm-PhBzAc.

Table 2. EL performances of OLEDs based on mCP, IpCm-PhBzAc, DpAn-BzAc and DpTrz-BphBzAc.

Devices	Maximum values				Values at 1000 cd/m ²				Values at 5000 cd/m ²				Values at 10000 cd/m ²			
	V _{on} (V)	CE (cd/A)	PE (lm/W)	EQE (%)	V (V)	CE (cd/A)	PE (lm/W)	EQE (%)	V (V)	CE (cd/A)	PE (lm/W)	EQE (%)	V (V)	CE (cd/A)	PE (lm/W)	EQE (%)
A1	4.7	27.8	10.4	7.6	6.1	19.4	10.2	5.3	8.6	25.1	9.3	6.9	10.1	27.6	8.5	7.4
A2	5.0	21.5	6.5	5.8	6.7	13.4	6.3	3.6	9.5	18.8	6.3	5.1	11.1	20.7	5.8	5.6
B1	2.2	54.4	70.4	15.5	3.2	49.4	49.1	14.0	4.6	46.4	31.2	13.0	6.1	44.3	22.8	12.6
B2	2.7	61.8	70.0	17.2	4.0	59.3	46.8	16.6	5.5	57.1	32.0	15.6	7.1	53.0	24.0	14.8
C1	2.3	40.1	48.9	11.1	3.1	39.3	40.3	10.8	3.9	35.8	29.2	9.8	4.5	33.3	23.3	9.3
C2	3.2	53.5	42.3	14.7	4.0	52.0	41.0	14.1	4.6	53.0	35.8	14.5	5.2	51.0	31.4	14.1

**Fig. 7** a) Luminance–voltage–current density. b) Current efficiency–luminance–EQE characteristics. c) EL spectra at 1000 cd m⁻² Inset: CIE coordinates of devices A2, B2 and C2.

Inspiringly, a promising result was also realized, in which the current efficiency roll-offs of devices B2 and C2 were suppressed by using the co-host EML. For example, at 5000 cd m⁻², the current efficiency of device B2 is moderately decreased to 57.1 cd A⁻¹. The current efficiency roll-off is 7.6%. As luminance increases to 10000 cd m⁻², the efficiency declines to 53.0 cd A⁻¹, while the roll-off is 14.2% exclusively. Remarkably, the co-host device C2 with mCP and DpTrz-BphBzAc in EML gives current efficiency of 53.0 cd A⁻¹ at 5000 cd m⁻², and the current efficiency roll-off is greatly reduced to 0.9%. The values at 10000 cd m⁻² are still kept high with CE of 51 cd A⁻¹ and efficiency roll-off of 4.7%. These results reveal that adding the mCP to the EML greatly decreases the triplet energy density, implying either triplet energy transfer from the co-host to the emitter and low probability of triplet-triplet exciton quenching. Hence, the efficiency roll-off is apparently mitigated. In addition, the host-dopant energy-transfer and carrier-trapping is available for exciton formation at high doping concentration. In particular, the exciton density of the T₁ state can be greatly reduced by converting the excitons from T₁ to the S₁ state through RSIC. The host material with TADF are beneficial for mitigating singlet-triplet annihilation (STA) and triplet-triplet annihilation (TTA), while STA and TTA are the main factors for the efficiency roll-off at high current densities. In addition, the novel host material with high carrier mobility can effectively reduce the driving voltage of the devices.

The above-mentioned results suggest that these BzAc derivatives are good green hosts and have potential applications in OLEDs with high luminance and high performance. Both of DpAn-BzAc and DpTrz-BphBzAc -based devices showed rather high current efficiency and limited efficiency roll-off. In contrast, the devices hosted by IpCm-PhBzA are found to perform poorer than those hosted by the other two analogues, which could be due to the lower carrier mobility and poor PLQY of IpCm-PhBzA than the others. In addition, the use of a mixed EML host was efficient to get improved efficiency roll-off in the triplet devices.

We have furthermore used DpAn-BzAc and DpTrz-BphBzAc as TADF emitters to fabricate fluorescent OLED, referred to Devices B3 and C3. The device structures was: ITO/ HAT-CN (10 nm)/NPB (50 nm)/TAPC (60 nm)/10 wt% DpAn-BzAc:mCP (Device B3) or 10 wt%

DpTrz-BphBzAc:mCP (Device C3) (40nm)/TPBi:TmPyPb(1:1 35 nm)/Liq (1 nm)/Al (100 nm). Figure S8 of the ESI[†] shows the device performance of Device B-3 and C-3. The highest current efficiency of 2.6 and 6.6 cd A⁻¹ for Devices B3 and C3 are obtained, respectively. In addition, the EL spectra of the DpAn-BzAc-based Device B3 contains two peaks 100 cd m⁻², where the peak at 525 nm is consistent with that of PL emission, and the peak at 532 nm may be ascribed to formation of the exciplex. While DpTrz-BphBzAc-based Device C3 with a peak at $\lambda_{\text{peak}} = 500$ nm is observed at 100 cd m⁻².

Conclusions

In conclusion, three new host molecules with acridine ring as electron-donating ligand were synthesized and fully characterized as hosts in PHOLEDs. All of these compounds show similar HOMO and triplet energy (2.7 eV in their thin films), but different electron-withdrawing ligands and their attachment to electron-donating BzAc moiety have a large effect on their thermal stability and carrier mobility. The compound DpTrz-BphBzAc exhibits superior thermal stability, excellent bipolar transport properties and a small ΔE_{ST} afforded efficient RISC, thus reducing the triplet density of the host for PHOLEDs. Using the newly synthesized hosts and co-host mCP, a series of green PHOLEDs with excellent performance and low efficiency roll-off at high brightness was fabricated. Particularly, the DpAn-BzAc based co-host device revealed the highest CE of 61.8 cd A⁻¹, the maximum EQE of 17.2%, and the co-host device of DpTrz-BphBzAc also gave CE of 53.5 cd A⁻¹ with low efficiency roll-off of 0.9% at 5000 cd m⁻². In addition, our PHOLED also presented a high power efficiency of 70.4 lm W⁻¹, which plays an important role in the reduction of power assumption for practical applications. These make BzAc derivatives promising hosts for high performance OLED and lighting applications at high luminance.

Experimental

General information

All chemicals and reagents were used as received from commercial sources without further purification unless stated otherwise. The auxiliary materials for OLED fabrication such as dipyrzino[2,3-f:20,30-h] quinoxaline 2,3,6,7,10,11-hexacarbonitrile (HAT-CN), NO-diphenyl-[1,10-biphenyl]-4, 40-diamine (NPB), 1,3-bis(9-carbazolyl)benzene (mCP), bis(2-phenylpyridine) iridium(III) acetylacetonate [(ppy)₂Ir(acac)], 1,1-bis[4-(di-p-tolylamino)phenyl]cyclohexane (TAPC), 1,3,5-tris(N-phenylbenzimidazol-2-yl) benzene (TPBi), 1,3,5-tri(m-pyrid-3-yl-phenyl)benzene (TmPyPB) and lithium quinolinolate (Liq) were purchased from Lumtec Luminescence Technology Corp.

Synthesis

3-(4-(12,12-Dimethylbenzofuro[3,2-b]acridin-7(12H)-yl)phenyl)-6-isopropyl-4H-chromen-4-one (IpCm-PhBzAc) :

3-(4-Bromophenyl)-6-isopropyl-4H-chromen-4-one (PhBzAc) (3.78 g, 11mmol), 5-phenyl-5,7-dihydroindolo[2,3-b]carbazole (2.99 g, 10mmol), Pd₂(dba)₃ (0.1 g, 0.11 mmol and potassium t-

butoxide (3.37 g, 30mmol) in toluene (100 mL) were stirred in a three-necked flask under a nitrogen atmosphere. The solution was then refluxed for 12 h. After cooling to room temperature, the solution was extracted with ethyl acetate and distilled water. The resulting residue was purified by column chromatography using petroleum ether/dichloromethane (5:1) to get the compound as a yellow powder (4.75 g, 84.6%). ¹H NMR (500 MHz, CDCl₃): 1.34-1.36 (d, *J* = 6.93 Hz, 6H), 1.80 (s, 6H), 3.06-3.14 (m, 1H), 6.45-6.47 (dd, *J*₁ = 8.14 Hz, *J*₂ = 1.28 Hz, 1H), 6.55 (s, 1H), 6.97-7.00 (td, *J*₁ = 7.47 Hz, *J*₂ = 1.29 Hz, 1H), 7.02-7.06 (td, *J*₁ = 7.62 Hz, *J*₂ = 1.66 Hz, 1H), 7.27-7.33 (m, 2H), 7.41-7.43 (dd, *J*₁ = 6.98 Hz, *J*₂ = 1.32 Hz, 1H), 7.47-7.50 (m, 3H), 7.52-7.54 (dd, *J*₁ = 7.58 Hz, *J*₂ = 1.59 Hz, 1H), 7.61-7.63 (dd, *J*₁ = 8.63 Hz, *J*₂ = 2.25 Hz, 1H), 7.87-7.89 (m, 1H), 7.90-7.92 (m, 2H), 8.00 (s, 1H), 8.19 (s, 1H), 8.21-8.22 (d, *J* = 2.23 Hz, 1H).

10-(4-(12,12-dimethylbenzofuro[3,2-b]acridin-7(12H)-yl)phenyl)-10-phenylanthracen-9(10H)-one (DphAn-BzAc)

5-phenyl-5,7-dihydroindolo[2,3-b]carbazole (2.99 g, 10mmol), 10-(4-bromophenyl)-10-phenylanthracen-9(10H)-one (DphAn-Br) (4.68 g, 11 mmol), Pd₂(dba)₃ (0.1 g, 0.11mmol) and potassium t-butoxide (3.37 g, 30 mmol) in toluene (100 mL) were stirred in a three-necked flask under a nitrogen atmosphere. The solution was then refluxed for 12h. After cooling to room temperature, the solution was extracted with ethyl acetate and distilled water. The organic layer was dried over anhydrous MgSO₄ and evaporated using a rotary evaporator. The resulting residue was purified by column chromatography using petroleum ether/dichloromethane (5:1) to get the compound as a yellow powder (5.36 g, 80%). ¹H NMR (500 MHz, CDCl₃): 1.75 (s, 6H), 6.32-6.34 (dd, *J*₁ = 8.06 Hz, *J*₂ = 1.25 Hz, 1H), 6.51 (s, 1H), 6.96-6.99 (m, 1H), 7.01-7.04 (td, *J*₁ = 7.70 Hz, *J*₂ = 1.59 Hz, 1H), 7.11-7.13 (m, 2H), 7.27-7.35 (m, 11H), 7.44-7.46 (dd, *J*₁ = 7.27 Hz, *J*₂ = 0.62 Hz, 1H), 7.50-7.54 (m, 3H), 7.59-7.63 (m, 2H), 7.87-7.88 (dd, *J*₁ = 7.28 Hz, *J*₂ = 1.28 Hz, 1H), 7.98 (s, 1H), 8.36-8.38 (dd, *J*₁ = 7.88 Hz, *J*₂ = 1.26Hz, 2H).

7-(4'-(4,6-Diphenyl-1,3,5-triazin-2-yl)-[1,1'-biphenyl]-4-yl)-12,12-dimethyl-7,12-dihydrobenzofuro[3,2-b]acridine (DpTrz-BphBzAc)

2-(4'-Bromo-[1,1'-biphenyl]-4-yl)-4,6-diphenyl-1,3,5-triazine (5.11 g, 11 mmol), (2.99 g, 10 mmol), 5-phenyl-5,7-dihydroindolo[2,3-b]carbazole, (3.37 g, 30mmol), potassium t-butoxide (0.1 g, 0.11 mmol), Pd₂(dba)₃ in toluene (100 mL) were stirred in a three-necked flask under a nitrogen atmosphere. The solution was then refluxed for 12 h. After cooling to room temperature, the solution was extracted with ethyl acetate and distilled water. The organic layer was dried over anhydrous MgSO₄ and evaporated using a rotary evaporator. The resulting residue was purified by column chromatography using petroleum ether/dichloromethane (5:1) to get the compound as a yellow powder (5.63 g, 82.5%). ¹H NMR (500 MHz, CDCl₃): 1.82 (s, 6H), 6.47-6.49 (dd, *J*₁ = 7.91 Hz, *J*₂ = 1.26 Hz, 1H), 6.57 (s, 1H), 6.99-7.03 (td, *J*₁ = 7.42 Hz, *J*₂ = 1.27 Hz, 1H), 7.04-7.08 (m, 1H), 7.28-7.34 (m, 2H), 7.42-7.43 (m, 1H), 7.52-7.56 (m,3H), 7.60-7.65 (m, 6H), 7.88-7.90 (m, 1H), 7.93-7.95 (m, 2H), 8.00-8.02 (m,3H), 8.83-8.84 (m, 4H), 8.93-8.95 (m, 2H).

Measurements

^1H NMR spectra were recorded on a Bruker AV-500 spectrometer at room temperature. High resolution mass spectra (HRMS) were determined on a Thermo Fisher Scientific LTQ FT Ultra mass spectrometer. UV-vis absorption spectra were recorded on a UV-2501PC instrument. Photoluminescence spectra were taken using a FLSP920 fluorescence spectrophotometer, both in solution and in the solid state. Cyclic voltammetry was carried out using a CH Instrument 660E electrochemical analyzer and with a Ag/AgCl electrode as the reference electrode, with tetra(n-butyl) ammonium hexa-fluorophosphate (TBAPF6) in DMF as the supporting electrolytes. The glass transition temperatures (T_g) of the compounds were determined under a nitrogen atmosphere using differential scanning calorimetry on a TA Q500 HiRes thermal analyzer with a scanning rate of $10\text{ }^\circ\text{C min}^{-1}$ with nitrogen flushing. The decomposition temperature corresponding to 5% weight loss was conducted on a TA Q500 HiRes TGA thermal analyzer.

Device fabrication and measurement

The devices were fabricated using conventional vacuum deposition of the organic layer and cathode onto an indiumtin-oxide (ITO) coated glass substrate under a base pressure lower than 5.0×10^{-5} mbar. Prepared glass substrates were cleaned using detergent, de-ionized water, acetone, and isopropanol. Immediately prior to loading into a custom-made high vacuum thermal evaporation chamber, the substrates were treated to a UV-ozone environment for 15 min. Then, organic layers and a metal cathode layer were evaporated successively by using shadow mask. The host complexes in the films were deposited on the glass substrates through thermal evaporation under a 5.0×10^{-5} mbar pressure to determine the PL spectrum and material characteristics. The entire organic layers and the Al cathode were deposited without exposure to the atmosphere. The deposition rates for the organic materials, and Al were typically 1.0 and 5.0 \AA s^{-1} , respectively. For the EML of co-deposited devices, three independent sources of mCP, novel material and (ppy) $_2$ Iracac were prepared. The three source were thermally evaporated together with the selected mass ratio 1:1:0.24. The current density–voltage–luminescence (J–V–L) characteristics were measured using FS-1000GA Test System. The luminance and spectra of each device were measured in the direction perpendicular to the substrate.

Acknowledgements

This work was financially supported by the Project of the National Science Foundation (Grant Nos. 51725505 and 61775130), “973” program (2015CB655005), and the Science and Technology Committee of Shanghai (15590500500).

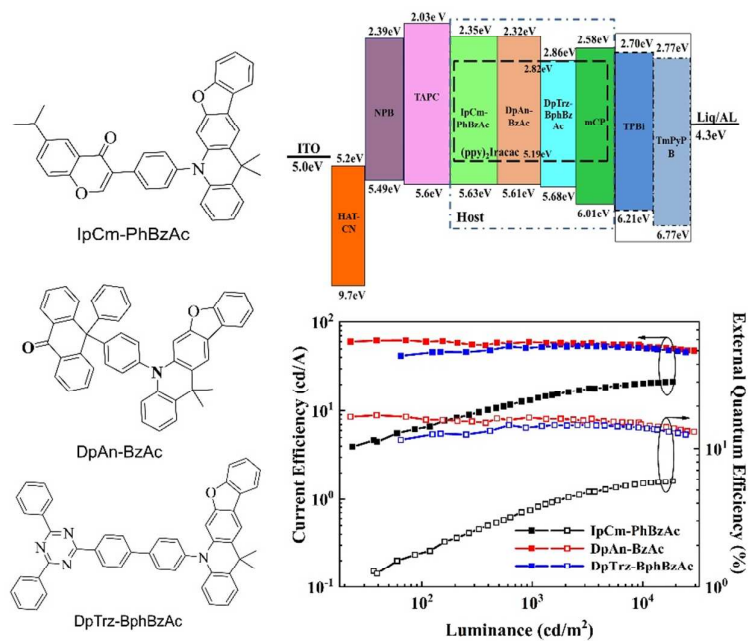
References

1. T.-H. Han, Y. Lee, M.-R. Choi, S.-H. Woo, S.-H. Bae, B. H. Hong, J.-H. Ahn and T.-W. Lee, *Nat. Photonics*, 2012, **6**, 105.
2. J. Y. Kim, T. Yasuda, Y. S. Yang and C. Adachi, *Adv. Mater.*, 2013, **25**, 2666.
3. M. Slawinski, M. Weingarten, M. Heuken, A. Vescan and H. Kalisch, *Org. Lett.*, 2013, **14**, 2387.
4. M. A. Baldo, D. F. O'Brien, Y. You, A. Shoustikov, S. Sibley, M. E. Thompson and S. R. Forrest, *Nature*, 1998, **395**, 151.
5. (a) M. A. Baldo, S. Lamansky, P. E. Burrows, M. E. Thompson and S. R. Forrest, *Appl. Phys. Lett.*, 1999, **75**, 4; (b) C. Adachi, R. C. Kwong, P. Djurovich, V. Adamovich, M. A. Baldo, M. E. Thompson and S. R. Forrest, *Appl. Phys. Lett.*, 2001, **79**, 2082; (c) Y. Chi and P.-T. Chou, *Chem. Soc. Rev.*, 2010, **39**, 638; (d) H. Yersin, A. F. Rausch, R. Czerwieniec, T. Hofbeck and T. Fischer, *Coord. Chem. Rev.*, 2011, **255**, 2622.
6. R. Liu, Y. Cai, J.-M. Park, K.-M. Ho, J. Shinar and R. Shinar, *Adv. Funct. Mater.*, 2011, **21**, 4744.
7. G. Williams, C. Backhouse and H. Aziz, *Electronics*, 2014, **3**, 43.
8. J. J. Guo, X. L. Li, H. Nie, W. W. Luo, S. F. Gan, S. M. Hu, R. G. Hu, A. J. Qin, Z. J. Zhao, S. J. Su, and B. Z. Tang, *Adv. Funct. Mater.*, 2017, 1606458.
9. T. Peng, G. M. Li, K. Q. Ye, S. Huang, Y. Wu, Y. Liu and Y. Wang, *Org. Electron.*, 2013, **14**, 1649.
10. W. Y. Hung, Z. W. Chen, H. W. You, F. C. Fan, H. F. Chen and K. T. Wong, *Org. Electron.*, 2011, **12**, 575.
11. M. A. Baldo, C. Adachi and S. R. Forrest, *Phys. Rev. B: Condens. Matter Mater. Phys.*, 2000, **62**, 10967.
12. S. Reineke, K. Walzer and K. Leo, *Phys. Rev. B: Condens. Matter Mater. Phys.*, 2007, **75**, 125328.
13. C. Murawski, K. Leo and M. C. Gather, *Adv. Mater.*, 2013, **25**, 6801.
14. C. H. Chen, L. C. Hsu, P. Rajamalli, Y.-W. Chang, F.-I. Wu, C.-Y. Liao, M.-J. Chiu, P.-Y. Chou, M.-J. Huang, L.-K. Chu and C.-H. Cheng, *J. Mater. Chem. C*, 2014, **2**, 6183.
15. T. Peng, G. M. Li, K. Q. Ye, S. Huang, Y. Wu, Y. Liu and Y. Wang, *Org. Electron.*, 2013, **14**, 1649.
16. Y. Tao, Q. Wang, C. Yang, Q. Wang, Z. Zhang, T. Zou, J. Qin and D. Ma, *Angew. Chem., Int. Ed.*, 2008, **47**, 8104.
17. Y. T. Tao, C. L. Yang and J. G. Qin, *Chem. Soc. Rev.*, 2011, **40**, 2943.
18. D. Kim, V. Coropceanu and J.-L. Brédas, *J. Am. Chem. Soc.* 2011, **133**, 17895.
19. A. Chaskar, H.-F. Chen and K.-T. Wong, *Adv. Mater.*, 2011, **23**, 3876.
20. A. Chaskar, H.-F. Chen, K.-T. Wong, *Adv. Mater.*, 2011, **23**, 3876.
21. H.-H. Chou and C.-H. Cheng, *Adv. Mater.*, 2010, **22**, 2468.
22. Y. Tao, K. Yuan, T. Chen, P. Xu, H. Li, R. Chen, C. Zheng, L. Zhang and W. Huang, *Adv. Mater.*, 2014, **26**, 7931.
23. K. Shizu, H. Noda, H. Tanaka, M. Taneda, M. Uejima, T. Sato, K. Tanaka, H. Kaji and C. Adachi, *J. Phys. Chem. C*, 2015, **119**, 26283.
24. H. Uoyama, K. Goushi, K. Shizu, H. Nomura and C. Adachi, *Nature*, 2012, **492**, 234.
25. W. L. Tsai, M. H. Huang, W. K. Lee, Y. J. Hsu, K. C. Pan, Y. H. Huang, H. C. Ting, M. Sarma, Y. Y. Ho, H.-C. Hu, C. C. Chen, M. T. Lee, K. T. Wong and C. C. Wu, *Chem. Commun.*, 2015, **51**, 13662.
26. M. Numata, T. Yasuda and C. Adachi, *Chem. Commun.*, 2015, **51**, 9443.
27. J. W. Suna, J. Y. Baekb, K.-H. Kima, J.-S. Huha, S.-K. Kwonb, Y.-H. Kim and J.-J. Kima, *J. Mater. Chem. C*, 2017, **5**, 1027.
28. S. Hirata, Y. Sakai, K. Masui, H. Tanaka, S. Y. Lee, H. Nomura, N. Nakamura, M. Yasumatsu, H. Nakanotani, Q. S. Zhang, K. Shizu, H. Miyazaki and C. Adachi, *Nat. Mater.*, 2015, **14**, 330.
29. B. Li, H. Nomura, H. Miyazaki, Q. S. Zhang, K. Yoshida, Y. Suzuma, A. Orita, J. Otera and C. Adachi, *Chem. Lett.*, 2014, **43**, 319.
30. Kazuo Udagawa, Hisahiro Sasabe, Fumiaki Igarashi, and Junji Kido, *Adv. Optical Mater.*, 2016, **4**, 86.
31. C. Murawski, K. Leo and M. C. Gather, *Adv. Mater.*, 2013, **25**, 6801.
32. Jin Won Sun, Jang Yeol Baek, Kwon-Hyeon Kim, Jin-Suk Huh, Soon-Ki Kwon, Yun-Hi Kim and Jang-Joo Kim, *J. Mater. Chem. C*, 2017, **5**, 1027.
33. Jeong-A Seo, Myoung-Seon Gong, Wook Song, and Jun Yeob Lee, *Chem. Asian J.*, 2016, **11**, 868.
34. K. Goushi, K. Yoshida, K. Sato, C. Adachi, *Nature Photonics*, 2012, **6**, 253-258

ARTICLE

Journal Name

35. J. Kalinowski, W. Stampor, J. Mezzyk, M. Cocchi, D. Virgili, V. Fattori and P. Di Marco, *Phys. Rev. B: Condens. Matter Mater. Phys.*, 2002, **66**, 235321.
36. Q.-L. Xu, X. Liang, S. Zhang, Y.-M. Jing, X. Liu, G.-Z. Lu, Y.-X. Zheng and J.-L. Zuo, *J. Mater. Chem. C*, 2015, **3**, 3694.



Optimal limited roll-off PhOLEDs are achieved based on acridine heterocyclic derivatives.